Molecular Basis of the Effects of Chloride Ion on the Acid−Base Catalyst in the Mechanism of Pancreatic α-Amylase†

Minxie Qian,‡ El Hassan Ajandouz,§ Françoise Payan,|| and Virginie Nahoum*,⊥

Department of Chemical Biology, State Key Laboratory for Structural Chemistry of Unstable and Stable Species, Peking University, Beijing 100871, People's Republic of China; Institut Méditerranéen de Recherche en Nutrition, UMR INRA−Université Aix Marseille III 1111, Faculté des Sciences et Techniques de Saint Jérôme, Case 342, Avenue Escadrille Normandie Niemen, 13397 Marseille, France; Architecture et Fonction des Macromolécules Biologiques, UMR 6098, CNRS and Universities Aix-Marseille I and II, 31 Chemin Joseph Aiguier, 13402 Marseille, France; and Centre de Biochimie Structurale, UMR5048 CNRS/UM1-UMR554 INSERM/UM1, Faculté de Pharmacie, BP14491, 15 Avenue Charles Flahault, 34093 Montpellier Cedex 5, France

Received August 19, 2004; Revised Manuscript Received November 9, 2004

ABSTRACT: Pig pancreatic α-amylase (PPA), an enzyme belonging to the α-amylase family, is involved in the degradation of starch. Like some other members of this family, PPA requires chloride to reach maximum activity levels. To further explain the mechanism of chloride activation, a crystal of wild-type PPA soaked with maltopentaose using a chloride-free buffer was analyzed by X-ray crystallography. A conspicuous reorientation of the acid/base catalyst Glu233 residue was found to occur. The structural results, along with kinetic data, show that the acid/base catalyst is maintained in the active site, in an optimum position, pointing toward the scissile bond−atom, due to the presence of chloride ions. The present study therefore explains the mechanism of PPA activation by chloride ions.

α-Amylase (α-1,4-glucan-4-glucanohydrolase, EC 3.2.1.1) catalyzes the hydrolysis of the α-(1,4)-glycosidic linkages in starch components, glycogen, and various oligosaccharides. α-Amylase is a member of family 13 of the sequenced-based classification of glycoside hydrolases, which is often termed the "α-amylase" superfamily (*1*) (CAZY website http://afmb.cnrs-mrs.fr/CAZY/). In mammals, α-amylase is present in both salivary and pancreatic secretions. Due to their central role in the starch degradation process, these enzymes are now being intensively investigated for fundamental, therapeutic, and diagnostic purposes. Although significant advances have been made, which help us to understand the reaction mechanism (*2*−*7*), some specific aspects of this mechanism still remain to be elucidated, especially as regards the role of chloride ion.

The three-dimensional structure of porcine (*8*, *9*) and human pancreatic α-amylases (*10*) (PPA and HPA, respectively)[1] are extremely similar, and so are their patterns of interaction with carbohydrate and proteinaceous inhibitors (*2*, *11*, *12*). PPA is an *endo*-type amylase, which catalyzes the hydrolysis of internal α-(1,4)-glucosidic bonds in amylose and amylopectin, resulting in the gradual degradation of the substrate toward the non-reducing end (*13*). The architecture of the pancreatic α-amylase (which is that of all the other enzymes belonging to the glycoside hydrolase family 13) consists of three domains: a catalytic core domain (A) comprising a $(\beta/\alpha)_8$ barrel, an extended loop inserted between the third β-strand and the third α-helix (called domain B, residues 100−169), and a C-terminal eight-stranded β-sheet domain (domain C, residues 405−496). Elements originating from domains A and B are involved in the architecture of the three most functionally important sites: the active site, the calcium binding site, and the chloride binding site. These enzymes catalyze glycoside hydrolysis via a double-displacement mechanism, basically as outlined by Koshland in 1953 (*14*). The two-step mechanism for retaining glycoside hydrolases requires the presence of two carboxyl-containing amino acids, one of which acting as an acid/base catalyst, and the other as the nucleophile responsible for the formation of the glycosyl-enzyme intermediate (*6*, *15*). In pancreatic α-amylase, Glu233 is the most appropriate candidate for the general acid which protonates the glycosidic oxygen of the scissile bond in the first step, and then deprotonates the attacking OH group in the second step. Asp197 is responsible for the nucleophile displacement of the aglycone forming the covalent linkage within the glycosyl-enzyme intermediate; structural and kinetic data have substantiated this assumption (*2*, *6*). Both the glycosylation and deglycosylation steps are thought to proceed through oxocarbenium ion-like transition states.

Several α-amylases, including the porcine pancreatic enzyme (*16*), the bacterial enzyme from *A.haloplanctis* (*17*)

† This work was funded by the CNRS; Program de Recherches Avancées de Cooperation Franco-Chinoise (PRA B95-4, Etudes Structurales) (M.Q. and F.P.), and the 863 High Technology Program of China.

* To whom correspondence should be addressed. Phone: 33 4 67 04 34 35; Fax: 33 4 67 52 96 23; E-mail: virginie@cbs.cnrs.fr.

‡ Peking University.

§ UMR INRA−Université Aix Marseille III 1111.

|| CNRS and Universities Aix-Marseille I and II.

⊥ UMR5048 CNRS/UM1-UMR554 INSERM/UM1.

[1] Abbreviations: PPA, pig pancreatic α-amylase; HPA, human pancreatic α-amylase; G5, maltopentaose; PPAII, pig pancreatic α-amylase isoform II; AHA, *Pseudoalteromonas haloplanctis* α-amylase.

10.1021/bi048201t CCC: $30.25
Published on Web 02/11/2005

and the insect enzyme from *Tenebrio molitor* larvae (*18*), have been found to require chloride to show full catalytic activity. In these α-amylases, the removal of chloride resulted in a significant decrease in activity (*16*, *19*). By contrast, most microbial α-amylases are not affected by the presence of chloride, which means that α-amylases can be classified as either chloride-dependent or chloride-independent enzymes (*20*). Structural studies have led to the detection of a chloride binding site in α-amylases from pig and human pancreas, from human saliva (*8*−*10*, *21*), from *Tenebrio molitor* larvae (*22*, *23*) and from the bacteria *P. haloplanctis* (*24*). These studies have shown that in the chloride-dependent α-amylases, there is a conserved chloride ion binding site located on the same side of the *β*-barrel as the catalytic site and the calcium binding site, in the vicinity of both, consisting of three residues Arg195, Arg337, Asn298 and a water molecule (*5*, *8*) (see diagram at 1.38 Å resolution, Figure 1A). The binding of chloride ion to mammalian α-amylases leads to an increase in the activities and a shift in the optimum pH from acidic values to neutrality (*16*, *19*). In our previous structural analysis of the complex formed between PPA and the acarbose inhibitor (*2*), we suggested that the observed shift in the pH-optimum may be attributable to the repulsion between the anion and the residue Glu233; the chloride ion is in the close vicinity of the *δ* carbon of E233. This interaction was expected to increase the pK_a of this residue and corroborated our idea that Glu233 acts as the proton donor. Numao et al. (2002) (*7*) have suggested that the chloride may be required to increase the pK_a of the acid/base catalyst Glu233, which would otherwise be lower due to the presence of Arg337, a positively charged residue. The authors of many previous studies (see also refs *9* and *25*) have assumed that the removal of chloride would affect the residue Glu233 (catalytic acid/base), but this hypothesis has not been proved directly. Here we present a structural study showing that the direct effects of chloride ions on the key catalytic glutamic acid carboxyl group are attributable to the fact that the chloride orients the side-chain of Glu233 to optimize the catalytic process.

MATERIALS AND METHODS

Preparation of Crystalline Complex. Native PPA crystals were grown at 4 °C as in our previous studies (*26*), from solutions of α-amylase in 10 mM Tris-HCL buffer. To induce an exchange between the structural chloride ion and the buffer, the complex described in the present study was formed by soaking the crystal for 1 h at 4 °C in a chloride-free solution containing 10 mM of G5 in phosphate buffer 20 mM at pH8, instead of using the usual buffer.

Data Collection and Processing. X-ray diffraction data were collected from a single crystal flash cooled in 30% ethylene glucose to 100K for data collection using a Mar-Research Imaging plate system and a rotating anode as X-ray source. The data were processed and scaled with the Denzo and Scalepack programs (*27*). The data collection statistics are summarized in Table 1.

Molecular Replacement and Refinement. The initial phases were calculated by molecular replacement using the AMoRe program (*28*) and the 2.2 Å structure of PPAII (*26*) as the starting model for the rigid body. The subsequent refinement procedure was performed using the CNS slow-cooling procedure (*29*) with all the data recorded between 35 and 2.02 Å. As all the data recorded were used in the refinement procedure, a low-resolution bulk solvent correction method implemented in the CNS program (*30*) was applied. The R_{free} behavior was monitored. Manual correction of the model using TURBO−FRODO (*31*), interspersed with slow cooling cycles, yielded a final *R*-factor of 0.159 (R_{free} = 0.184).

Table 1: Refinement and Structure Quality Statistics

Data quality	
resolution of data (outer shell) (Å)	25−2.02 (2.07−2.02)
no. of measurements	224738 (12647)
no. of unique reflections	61363 (4199)
R_{merge} (outer shell)[a]	0.067 (0.173)
completeness (outer shell) (%)	98.6 (98.6)
multiplicity (outer shell)	3.7 (3.0)
data > 1σ (%)	98.32 (95.99)
Refinement	
space group	$P2_12_12_1$
cell parameters: *a*; *b*; *c* (Å)	70.090; 113.298; 117.221
no. protein atoms; discretely disordered residues	3960; 5
no waters; ligand atoms; ethylene glycol atoms	749; 91; 24
no. of ion atoms	2 ($1Ca^{2+}$; $0.35Cl^-$)
resolution used in refinement (Å)	35.0−2.02 (2.05−2.02)
R_{cryst}[b] (outer shell)	15.91 (17.59)
R_{free} (outer shell)	18.38 (21.35)
mean *B* (Å^2) for protein atoms; main-chain; side-chain	16.44; 12.84; 19.06
mean ligand atoms *B* (Å^2) (active site)	26.75
(subsite)	25.87(−1); 24.33(−2); 30.14(−3)
mean ligand atoms *B* (Å^2) (surface site)	33.15
B value (Wilson plot) (Å^2)	20.98
rms deviation of bonds (Å)	0.007
rms deviation of angles (deg)	1.38
rms deviation of impropers (deg)	1.255

[a] $R_{merge} = \sum_h\sum_i|I_{h,i} - \langle I_h\rangle|/\sum_h\sum_i|I_{h,i}|$. [b] R_{cryst} is defined as $\sum|F_o - F_c|/\sum|F_o|$.

More specifically, the refinement procedure was carried out starting with the refined structure of free PPA, and deleting the water molecules, which overlapped with the observed initial difference Fourier density. The template of a glucose residue used for the refinement of the ligand structure was based on crystallographic data on individual monosugars. Solvent molecules with densities below 1σ in the $2F_o - F_c \exp(i\alpha_c)$ ML-weighted map and a temperature factor above 55 Å^2 were removed after the first refinement step. The difference electron density map also showed the presence of additional water molecules, although some of the ordered molecules previously present in the free enzyme structure had disappeared. The new water molecule sites were added to the model whenever the electron density level was at least 3.5σ in the $F_o - F_c \exp(i\alpha_{cal})$ maps. The molecules introduced were inspected visually to check whether the hydrogen-bonding geometry was correct, and they were given an initial B factor of 20 Å^2. No oligosaccharide atoms were included in the model until the refinement of the protein had reached convergence. During the *B* value refinement procedure, the oligosaccharide molecules were refined with no restraints on the *B* value.

Interestingly, in addition to the presence of an electron density patch at the active site corresponding to a maltotriose entity bound to subsites −3 through −1, the initial difference Fourier map calculated without chloride ions clearly and

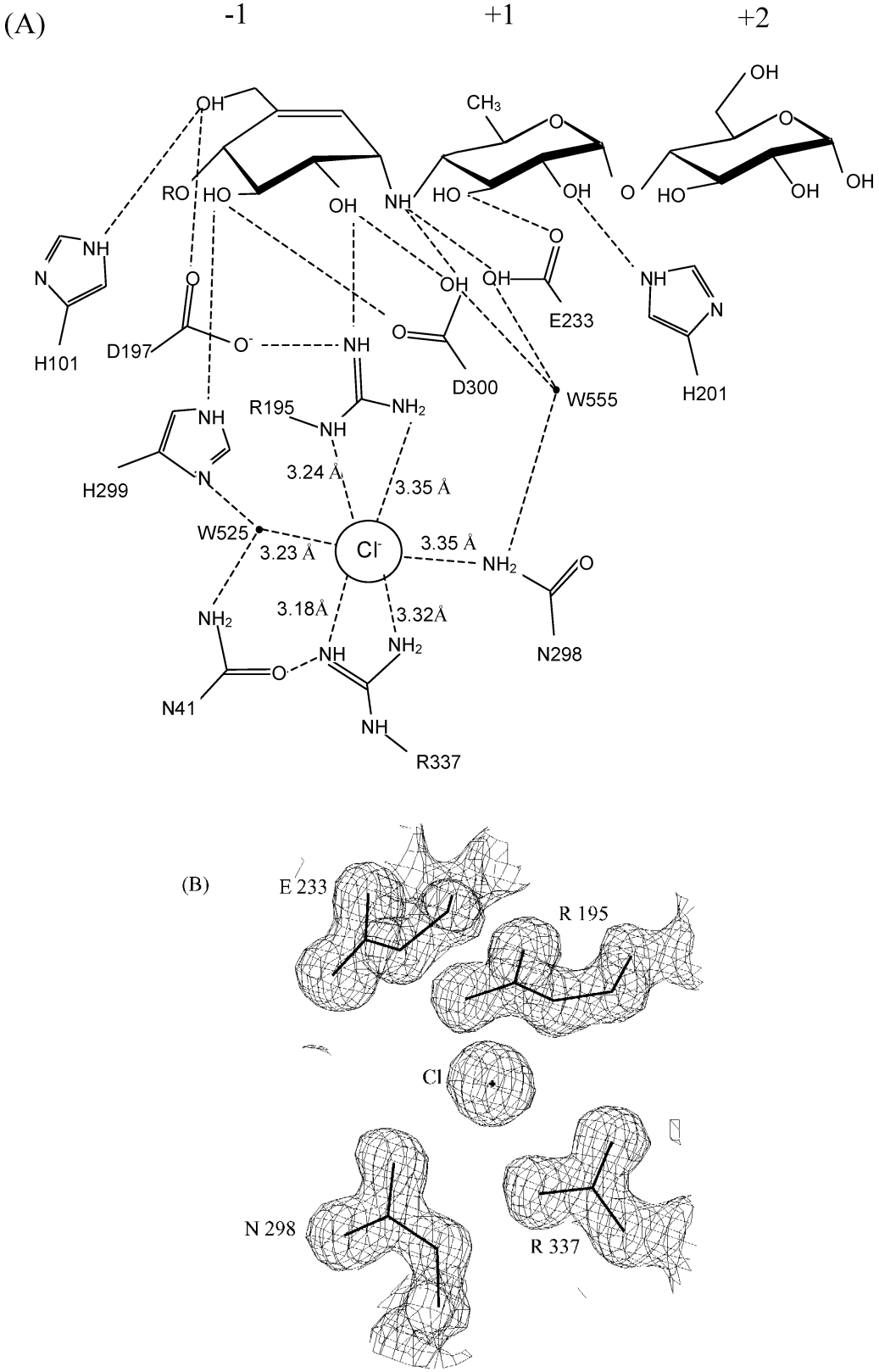

FIGURE 1: (A) Schematic representation at 1.38 Å of the network of interactions within the chloride binding site, the neighboring catalytic center and the bound acarbose-derived inhibitor, (adapted from ref 5). For the sake of clarity, only subsites −1, +1, +2 of the bound ligand are shown. Dashed lines give distances shorter than 3.5 Å. (B) Close-up view showing the $2F_o - F_c$ electron density pattern (1.5σ contoured) observed within the chloride binding site in the structure of PPA/acarviosine complex in the presence of chloride at 1.38 Å resolution (5).

unambiguously showed the presence of strong structural changes in the catalytic center. The electron density landscape in this area was different from that observed in previous studies (see Figure 1B), particularly as far as the catalytic residue Glu233 and the chloride ions were concerned: a strong positive continuous V-shaped $F_o - F_c$ electron density extending beyond the CB atom of Glu233 toward the position of the normally bound chloride ion was observed. The clear-cut shape of this initial electron density patch unambiguously accounted for the atoms of the Glu233 side-chain beyond

the CB and indicated that the catalytic residue was present in a new orientation. Although this extra positive V-shaped $F_o - F_c$ density was topped by a positive ball of electron density in the position where Cl^- normally stands, it was clearly less strong than the electron density patch usually observed in this position in the case of the structural chloride ion (A chloride ion electron density map is shown in Figure 1B). As expected, when a chloride ion with full occupancy was included in the refinement procedure, the resulting $F_o - F_c$ map showed a negative density peak in this position. Interestingly, the positive electron density patch occurring between the chloride ion and the CB of Glu233 was still strongly present. The side-chain of Glu233 could be easily accommodated in this electron density patch; it was strongly rotated from the classical position of the acid/base catalyst oriented in an appropriate way for catalysis. The subsequent refinement procedure indicated that the residue was present in the structure with two alternative conformations: Alt1 (with an occupancy of 0.35), corresponding to the classical structure in which the chloride ion is present and the side-chain of Glu233 is turned toward the scissile bond−atom, and Alt2, the new rotated orientation (with an occupancy of 0.65) (Figure 2A). The chloride ion was introduced with a partial occupancy, and the electron density pattern observed resulted from coexisting states in the crystal. This model led to the best *R*-factor. The final refinement statistics obtained are given in Table 1. Coordinates have been deposited with the Brookhaven Protein Data Bank (accession code 1WO2) (*32*).

Kinetic Assays. Homogeneous PPA was purified from porcine pancreas as previously described (*33*), except that quaternary methylamine was used as the anion exchanger instead of diethylaminoethyl cellulose. The last purification steps were conducted in 10 mM Tris-HCl pH 8 containing 10 mM NaCl, 1 mM $CaCl_2$, 1 mM NaN_3 and 20 μM phenylmethylsulfonyl fluoride (inhibitor serine proteases). The enzyme was stored in this buffer and its concentration determined on the basis of its extinction coefficient at 280 nm, $A_{1\%(w:v)} = 25$ (*33*). Kinetic assays on maltopentaose were carried out at 30 °C in 20 mM sodium phosphate pH 6.9 containing 6 mM NaCl or not. These assays were repeated using chloride-free PPA, which was prepared by dialyzing the enzyme for 48 h against deionized water, with water replacement at 24 h. The reaction was initiated by adding PPA at 1.5 nM (at a roughly 10^5-fold dilution of the stock solution in phosphate buffer) to the buffer containing the substrate G5 at 500 μM (saturating concentration) (*34*). Samples were then collected at appropriate intervals (15, 30, 45, and 60 s), mixed with NaOH 0.1 M (three volumes) to stop the reaction and then kept on ice. The G5 concentration in these samples, as well as the concentrations of the products released (maltose and maltotriose), were determined using high-performance anion exchange chromatography coupled with pulsed amperometric detection (Dionex Corp., Sannyvale, CA), as described elsewhere (*34*). The initial rate of G5 hydrolysis was calculated from the linear regression of its disappearance in the 0−60 s interval (linear part of the curve) and the catalytic constant (initial velocity/concentration of enzyme, s^{-1}) was then obtained. All the kinetic determinations were at least duplicated and the values given (corresponding to standard deviations of less than 10%) are means.

RESULTS AND DISCUSSION

Evidence That Chloride Ion Has Direct Effects on the Acid/Base Catalyst: Structure of a PPA Crystal Soaked with Maltopentaose in a Cl^--Free Buffer. In Figure 1A, the structural elements and details of the interactions involved in the formation of the chloride ion binding site in the fully active PPA are shown at a resolution of 1.38 Å (*8*). It is worth noting that two positively charged side-chains (Arg195 and Arg337) interact directly here with the chloride ion.

The structure of "chloride-free" PPA was determined based on native PPA (including the structural chloride ion), but in this case, reacting the enzyme with a maltopentaose substrate in a chloride-free buffer. The crystal structure of the complex was determined using molecular replacement methods and the AMoRe program (see Materials and Methods) (*28*). The electron density map (see Figure 2A) shows the occurrence of a strong electron density patch corresponding to an unprecedented conformation of the acid/base catalyst. The present structural analysis clearly shows that a significant rearrangement of the side-chain of the acid/base catalyst Glu233 occurred. The key residue has changed its orientation, required for the catalysitic process, turning away from the cleavage point and projecting into the chloride binding site (see Figure 2B). As a result, the carboxyl group is observed in H-bonding with the positively charged arginine side-chains of the chloride binding site (Arg195 and Arg337). This shows that the acid/base catalyst is held in the active site by the chloride ion, in the optimum position, pointing toward the scissile glycosidic bond. When the chloride ion is incorporated, Glu233 is therefore obviously shielded by the negatively charged ion from the direct effects of Arg195 and Arg337.

This finding helps to explain a number of previous data on the relations between the key residue Arg195, the chloride ion and the acid/base catalyst Glu233. The resolution of the Arg195 mutant HPA structure (*7*) showed that the substitution of Arg195 by an alanine (or even by a glutamine) causes little perturbation of the main chain conformation; it leads, however, to the loss of ability of HPA to bind to chloride ion (which results in a 450-fold decrease in the activity in comparison with the wild type HPA), but only a slight shift of Glu233 was observed within the active site. Likewise, the Arg337 mutant HPA structures (*7*) indicated that only a few structural changes have occurred in the mutant (some very slight changes were observed in the side-chains of Arg195, Glu233, Asp300) despite the removal of a large charged internal side-chain, as well as an internally bound chloride ion. In the present structure, on the contrary, the removal of the chloride ion induces a drastic structural change in the Glu233 side-chain, which moved far away from the catalytic center toward the location of the normally bound chloride. In our experiments, the chloride ions were removed via the exchange (from the crystal to the chloride-free buffer) induced by the chloride-concentration gradient; the positive charges of the arginines kept their native position. Therefore, the Glu233 side-chain changed its catalytic position to interact with the arginine positive charges, while in the previous study (*7*), the removal of the positively charged residues resulted in the loss of the chloride ion but failed to induce the acid/base catalyst reorientation, a water molecule was found at the location of the normally bound ion. The

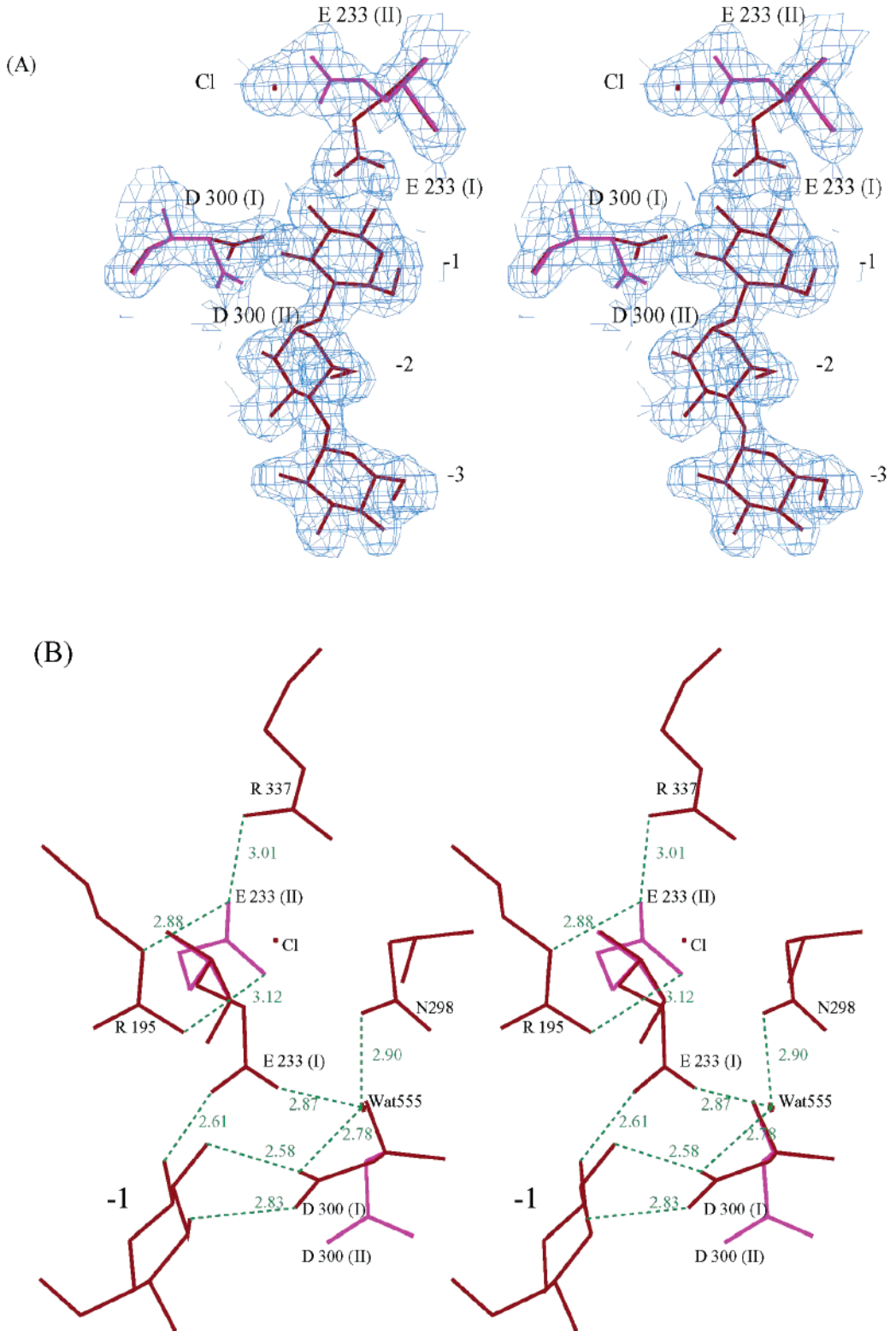

FIGURE 2: (A) Stereoview of the final $(2F_o - F_c)\exp(i\alpha_c)$ electron-density map (1σ contoured) observed within the chloride binding site and the neighboring part of the catalytic center, when the crystal is immersed in a solution of maltopentaose devoid of chloride ions. Alternative conformations Alt1 (in red) and Alt2 (in pink) (see Materials and Methods section) are numbered (I) and (II), respectively. (B) Detailed Stereoview of the arrangement of protein side-chains involved in the chloride binding site in a crystal of PPA soaked with maltopentaose in a Cl^--free buffer. The rotated position (colored pink) of the acid/base catalytic residue Glu233 and its H-bonding interactions with Arg195 and Arg337 can be seen. The putative intervening water (555) is shown. Sugar units bound at subsites −2 and −3 have been omitted for the sake of clarity.

removal of the side-chain of the critical chloride ligands, which results in the loss of the chloride ion, therefore has completely different effects from the removal of the chloride from the native enzyme. Here we have strong experimental evidence that the presence of the chloride ion is necessary to oppose the action of the arginine side-chains and maintain Glu233 in its optimum position with an optimum charge at the physiological pH (neutral pH). In mammalian α-amy-

lases, the presence of chloride ions is a decisive factor for Glu233 to adopt the appropriate orientation for maximum enzyme activity to occur.

The present results may also allow provide a new explanation for the structural data published on the chloride-free mutant Lys300Gln-AHA (*25*). In all the chloride-dependent α-amylase crystal structures solved so far, the anion binds to a common site. In the α-amylase from *P. haloplanktis* (AHA), the corresponding chloride ligands are Lys300 (Arg337 in PPA notation), Arg172 (195), Asn262 (298), and H_2O1003 (252). In the structural study by Aghajari et al., it was established that the mutation of the critical chloride ligand Lys300 into a glutamine resulted in an active but chloride-independent enzyme. The absence of chloride in the Lys300Gln-AHA structure was clearly seen from the crystallographic results. This finding led the authors to conclude that the chloride ion was not essential to the catalytic mechanism. However, our results suggest that the presence of the non polar Gln side-chain at the mutated anion binding site failed to induce the rotation of the catalytic acid/base residue away from its functional position, which would explain why no change was observed in the activity of the chloride-free mutant.

It is 30 years now since the pioneering work by Levitzki and Steer (*16*) suggested the importance of the physiological effector ligand: the chloride ion. The latter authors observed that, with very different substrates such as starch and *p*-nitrophenylmaltoside (which is a less effective substrate than starch), the degree of activation were identical. They therefore assumed that the chloride effector might exert its activity on common catalytic steps (rather than being involved in the multirepetitive attacks which are system specific to PPA), resulting in the formation of the glycosyl enzyme and its hydrolysis. They also concluded that Cl^- induced a subtle conformational change at some crucial, as yet unknown site inducing large catalytic accelerations. The idea that Cl^- may have an orienting effect on the catalytic groups at the active site was also put forward at that time.

Interestingly, the results of the present study, showing that the chloride ion acts on the orientation of the acid−base catalyst, are in good agreement with these suggestions and elucidate all these points many years after they were first put made.

It is also worth noting that the present structure shows that the general fold of the chloride binding region is not affected by the lack of chloride ions, in agreement with previous studies (see ref *7*). The chloride ligands, as well as the nucleophile Asp197, remain unchanged when the structural ion is not incorporated. The active site water molecule, which was identified earlier as a molecule possibly participating in the acid/base catalytic step (Wat 555 in pdb entry code 1PPI, ref *2*), is still present and continues to be involved in H-bonding interactions with the chloride ligand Asn298, while the interactions with the rotated side-chains of Glu233 (and Asp300) are lost.

It is worth mentioning here that the native PPA crystal initially includes a structural chloride ion. As previously observed in the case of PPA (*16*), AHA (*17*), and HPA (*7*), these α-amylases in the state of chloride depletion display a low level of basal activity, and the activity of the enzyme depends on the chloride concentration in an approximately hyperbolic fashion. Under our experimental conditions (when the crystal is immersed in a solution devoid of chloride ions), the structural ion is largely removed. It is widely recognized that the crystal may constitute a mixture of coexisting states: in most of its molecules, the Cl^- ion has been removed and the carboxyl group of Glu233 replaces the anion (see Material and Methods section). Three additional surface chloride ions located in the vicinity of the active site were identified in the high-resolution study on PPA (*5*). Due to the lack of chloride ions in the medium, these surface chloride ions were replaced by water molecules in the present structure, as was to be expected. These points were confirmed by the refinement procedure. To address the role of the chloride in the phosphate buffer used in our crystallographic experiments, a complementary kinetic experiment was conducted both with and without chloride incorporated in the reaction medium. When the kinetic assay with native PPA was performed in the presence of 6 mM sodium chloride, the substrate was readily hydrolyzed with a kcat of 883 s^{-1}. Interestingly, when the assay was done in a chloride-free buffer, the kcat value decreased to 86 s^{-1}, showing that chloride-free α-amylase had a low level of activity. Similar results were obtained when extensive dialysis was performed to remove the chloride from the starting enzyme and the assay was performed in the presence of chloride: maximum activity levels (926 s^{-1}) were recorded in this case, but again, when the buffer contained no chloride ions, only about 10% of this activity (83 s^{-1}) was observed. The dramatic decrease in native PPA activity, which dropped from 883 s^{-1} in the chloride- containing buffer to 86 s^{-1} in the chloride-free buffer in our experiments, suggests that the chloride moved in the opposite direction, i.e., from the enzyme to the medium. This finding shows that the chloride ion is variably available, depending on the environmental conditions. It is worth noting that these data are in keeping with earlier results published by Feller et al., (*20*), who stated that the activity of chloride-dependent α-amylases can be modulated by varying the Cl^- concentration in the medium. The basal activity levels (observed with enzyme and medium devoid of chloride) amounting to 10% in the present study may have been due to either residual bound chloride, experimental deviations, contamination of water by chloride or may have been simply some other basal activity not dependent on chloride). All in all, the kinetic data obtained in the present study are in line with the structural events observed in the absence of chloride in the reaction medium. The crystals used in the crystallographic study were not obtained from a dialyzed enzyme, but grown from fully active native enzymes. In our experiment, they therefore continued to show more significant chloride occupancy values than what was suggested by the kinetic experiments on chloride-free PPA.

Active-Site Bound Ligand. The electron density pattern observed in the active site depression clearly indicates that a maltotriose entity remained bound to subsites −3 through −1. The three-dimensional structure of the product complex was recently analyzed in a crystallographic study on native PPA prepared under favorable conditions (pH 7 and structural ions incorporated), soaked and flash frozen with a maltopentaose substrate (*35*). In this study, the reaction product was found to bind at subsites −3, −2, and −1. In the present study, the reaction product also bound at subsites −3, −2, and −1, but interestingly, contrary to what occurred in the

previous study, the −1 subsite sugar gave an extremely well-defined electron-density patch. This difference observed at subsite −1 was due to the lack of activity which occurs after removing the chloride ion, since the substrate is converted only very slowly. Therefore, contrary to what occurred with an active crystalline enzyme, with which a mixture of possible conformations might coexist at subsite −1 (and yield disorder and weak density levels), the −1 sugar was found in the present structure to have a nondeformed chair conformation giving rise to an extremely well-defined pattern of electron density.

The first results clearly showing that chloride is involved in the kinetic behavior of a mammalian α-amylase were published by Levitzki and Steer in 1974 (*16*). Later studies have shown that this occurs not only in mammalian α-amylases, but also in distant living organisms (see ref *20*). Some relevant kinetic and structural data have been published on the role of the chloride ion, especially by authors using α-amylase mutants. Here we present a definite answer to the questions raised by Levitzki and Steer. The present results show the strong dependence of the acid/base catalyst on the environmental chloride, which by acting on the state of protonation of the catalyst, determines the activity of the α-amylase. This provides an explanation for the relationship between the specificity of the amino acid residues which form the chloride binding region and the activity of chloride-dependent α-amylases. The present study also sheds light on previous data on PPA, HPA, and AHA; all in all, these results suggest the general pattern of behaviour (in terms of the chloride effector) of chloride-dependent α-amylases. This links up with the suggestion made by Feller et al. (*20*) that corresponding engineering strategies should be developed. By performing a single amino acid substitution, it might be possible to transform chloride-independent α-amylases into chloride-dependent enzymes, thus opening a possible path towards modulating the enzyme activity by varying the Cl^- concentration in the medium.

ACKNOWLEDGMENT

We are grateful to Dr. Stefan Arold for useful discussions and for his critical reading of the manuscript.

REFERENCES

1. Henrissat, B. (1991) A classification of glycosyl hydrolases based on amino acid sequence similarities, *Biochem. J. 280*, 309−316.
2. Qian, M., Haser, R., Buisson, G., Dúee, E., and Payan, F. (1994) The active center of a mammalian alpha-amylase. Structure of the complex of a pancreatic alpha-amylase with a carbohydrate inhibitor refined to 2.2-A resolution, *Biochemistry 33*, 6284−6294.
3. McCarter, J. D., and Withers, S. G. (1996) Unequivocal identification of Asp-214 as the catalytic nucleophile of *Saccharomyces cerevisiae* alpha-glucosidase using 5-fluoro glycosyl fluorides, *J. Biol. Chem. 271*, 6889−6894.
4. Uitdehaag, J. C., Mosi, R., Kalk, K. H., Van der Veen, B. A., Dijkhuizen, L., Withers, S. G., and Dijkstra, B. W. (1999) X-ray structures along the reaction pathway of cyclodextrin glycosyltransferase elucidate catalysis in the alpha-amylase family, *Nat. Struct. Biol. 6*, 432−436.
5. Qian, M., Nahoum V., Bonicel J., Bischoff, H., Henrissat, B., and Payan, F. (2001) Enzyme-catalyzed condensation reaction in a mammalian alpha-amylase. High-resolution structural analysis of an enzyme−inhibitor complex, *Biochemistry 40*, 7700−7709.
6. Rydberg, E. H., Li, C., Maurus, R., Overall, C. M., Brayer, G. D., and Withers, S. G. (2002) Mechanistic analyses of catalysis in human pancreatic alpha-amylase: detailed kinetic and structural studies of mutants of three conserved carboxylic acids, *Biochemistry 41*, 4492−4502.
7. Numao, S., Maurus, R., Sidhu, G., Wang, Y., Overall, C. M., Brayer, G. D., and Withers, S. G. (2002) Probing the role of the chloride ion in the mechanism of human pancreatic alpha-amylase, *Biochemistry 41*, 215−225.
8. Qian, M., Haser, R., and Payan, F. (1993) Structure and molecular model refinement of pig pancreatic alpha-amylase at 2.1 A resolution, *J. Mol. Biol. 231*, 785−799.
9. Larson, S. B., Greenwood, A., Cascio, D., Day, J., and McPherson, A. (1994) Refined molecular structure of pig pancreatic alpha-amylase at 2.1 A resolution, *J. Mol. Biol. 235*, 1560−1584.
10. Brayer, G. D., Luo, Y., and Withers, S. G. (1995) The structure of human pancreatic alpha-amylase at 1.8 A resolution and comparisons with related enzymes, *Protein Sci. 4*, 1730−1742.
11. Nahoum, V., Roux, G., Anton, V., Rougé, P., Puigserver, A., Bischoff, H., Henrissat, B., and Payan, F. (2000) Crystal structures of human pancreatic alpha-amylase in complex with carbohydrate and proteinaceous inhibitors, *Biochem. J. 346*, 201−208.
12. Brayer, G. D., Sidhu, G., Maurus, R., Rydberg, E. H., Braun, C., Wang, Y., Nguyen, N. T., Overall, C. M., and Withers, S. G. (2000) Subsite mapping of the human pancreatic alpha-amylase active site through structural, kinetic, and mutagenesis techniques, *Biochemistry 39*, 4778−4791.
13. Robyt, J. F., and French, D. (1970) The action pattern of porcine pancreatic alpha-amylase in relationship to the substrate binding site of the enzyme, *J. Biol. Chem. 245*, 3917−3927.
14. Koshland, D. E. (1953) Stereochemistry and the Mechanism of Enzymatic Reactions, *Biol. Rev. 28*, 416−436.
15. McCarter, J. D., and Withers, S. G. (1994) Mechanisms of enzymatic glycoside hydrolysis, *Curr. Opin. Struct. Biol. 4*, 885−892.
16. Levitzki, A., and Steer, M. L. (1974) The allosteric activation of mammalian a-amylase by chloride, *Eur. J. Biochem. 41*, 171−180.
17. Feller, G., Bussy, O., Houssier, C., and Gerday, C. (1996) Structural and functional aspects of chloride binding to Alteromonas haloplanctis alpha-amylase, *J. Biol. Chem. 271*, 23836−23841.
18. Buonocore, V., Poerio, E., Silano, V., and Tomasi, M. (1976) Physical and catalytic properties of alpha-amylase from *Tenebrio molitor* L. Larvae, *Biochem J. 153*, 621−625.
19. Wakim, J., Robinson M., and Thoma, J. A. (1969) The active site of porcine pancreatic α-amylase: Factors contributing to catalysis, *Carbohydr. Res. 10*, 487−503.
20. D'Amico, S., Gerday, C., and Feller, G. (2000) Structural similarities and evolutionary relationships in chloride-dependent alpha-amylases, *Gene 253*, 95−105.
21. Ramasubbu, N., Paloth, V., Luo, Y. G., Brayer, G. D., and Levine, M. J. (1996) Structure of human salivary α-amylase at 1.6 Angstrom resolution: implications for its role in the oral cavity, *Acta Crystallogr. D52*, 435−446.
22. Strobl, S., Maskos, K., Betz, M., Wiegand, G., Huber, R., Gomis-Rüth, F. X., and Glockshuber, R. (1998) Crystal structure of yellow meal worm alpha-amylase at 1.64 A resolution, *J. Mol. Biol. 278*, 617−628.
23. Nahoum, V., Farisei, F., Le-Berre-Anton, V., Egloff, M. P., Rougé, P., Poerio, E., and Payan, F. (1999) A plant-seed inhibitor of two classes of alpha-amylases: X-ray analysis of *Tenebrio molitor* larvae alpha-amylase in complex with the bean Phaseolus vulgaris inhibitor, *Acta Crystallogr. D55*, 360−362.
24. Aghajari, N., Feller, G., Gerday, C., and Haser, R. (1998) Crystal structures of the psychrophilic alpha-amylase from Alteromonas haloplanctis in its native form and complexed with an inhibitor, *Protein Sci. 7*, 564−572.
25. Aghajari, N., Feller, G., Gerday, C., and Haser, R. (2002) Structural basis of alpha-amylase activation by chloride, *Protein Sci. 11*, 1435−1441.
26. Gilles, C., Astier J. P., Marchis-Mouren, G. Cambillau, C., and Payan, F. (1996) Crystal structure of pig pancreatic alpha-amylase isoenzyme II, in complex with the carbohydrate inhibitor acarbose, *Eur. J. Biochem. 238*, 561−569.
27. Otwinowski, Z. (1993) In *Data Collection and Processing: proceedings of the CCP4 study weekend* (Sawyer, L., Issacs, N., and Bailey, S., Eds) Science and Engineering Research Council, Daresbury, U.K.
28. Navaza, J. (1992) AMoRe: A new package for molecular replacement, In *Proceedings of the CCP4 Study Weekend* (Dodson,

E. J., Grower, S., and Wolf, W., Eds.), Science and Engineering Research Council, London. 87−91.
29. Brünger, A. T., Kuriyan, J., and Karplus, M. (1987) Crystallographic R factor refinement by molecular dynamics, *Science 35*, 458−460.
30. Brünger, A. T., Adams, P. D., Clore, G. M., DelLano, W. L., Gros, P., Grosse-Kunstleve, R. W., Jiang, J. S., Kuszewski, J., Nilges, M., Pannu, N. S., Read, R. J., Rice, L. M., Simonson, T., and Warren, G. L. (1998) Crystallography & NMR system: a new software suite for macromolecular structure determination, *Acta Crystallogr. D54*, 905−921.
31. Roussel, A., and Cambillau, C. (1989) In *Silicon Graphic Geometry Partner Directory*, (Fall, 1989), Silicon Graphics, Mountain View CA, 77−78.
32. Bernstein, F. C., Koetzle, T. F., Williams, G. J., Meyer, E. F., Jr., Brice, M. D., Rodgers, J. R., Kennard, O., Shimanouchi, T., and Tasumi, M. (1977) The Protein Data Bank: a computer-based archival file for macromolecular structures, *J. Mol. Biol. 112*, 535−42.
33. Cozzone, P., Pasero, L., and Marchis-Mouren, G. (1970) Caracterization of porcine pancreatic isoamylases: separation and amino acid composition, *Biochim. Biophys. Acta 200*(3), 590−3.
34. Al Kazaz, M., Desseaux, V., Marchis-Mouren, G., Prodanov, E., and Santimone, M. (1998) The mechanism of porcine pancreatic alpha-amylase. Inhibition of maltopentaose hydrolysis by acarbose, maltose and maltotriose, *Eur. J. Biochem. 252*, 100−7.
35. Payan, F., and Qian, M. (2003) Crystal structure of the pig pancreatic alpha-amylase complexed with malto-oligosaccharides, *J. Protein 22*, 275−284.

BI048201T